Multi-Objective Co-Design of Cell-to-Pack Battery Electric Vehicle Systems for Range, Cost, and Lifetime

Assyr Abdulle[1,*] and Bernard Louis Koff[2]

[1] Professor of Mathematics, EPFL; Mathematics Section, École Polytechnique Fédérale de Lausanne.
[2] Emeritus University Professor of Mathematical Sciences, Kent State University; adjunct professor at Case Western Reserve University.
* Correspondence: assyr.abdulle@epfl.ch

Abstract: Pack architecture emerges as a critical design parameter in battery electric vehicles, since it establishes the dominant fraction of the cost, usable range, pack weight, thermal load, and servicing value of the system. The present work develops a discrete multi-objective model for selecting pack architectures in cell-to-pack BEV systems, focusing on the evaluation of range, battery cost, and degradation cost per kilometre at the vehicle level. The candidate pool consists of 864 different pack architectures, created from the combination of two technology generations (2025 and 2030), three cell geometries, four gross energy classes, four levels of structural integration, three fast-charging rates, and three cycle lives. Cell-level density parameters are transformed into pack mass and volume, gross energy into usable energy, range is determined based on a mass-dependent consumption correlation, and lifetime is quantified in service-equivalent distance travelled at the end of life. Filtering candidates based on charging time, pack mass and volume limits leaves 747 candidate packs, while excluding redundant charge rates reduces the number of feasible architecture-lifetime combinations to 249. These results address the fundamental design question head-on by indicating that the largest battery does not yield optimal system performance in the representative C-segment crossover application. The optimum compromise design of 2025 technology consists of a 65 kWh prismatic pack at $\psi = 1.15$ with 2500 cycles, while the 2030 optimum has a capacity of 75 kWh with identical architecture parameters. High levels of integration and long cycle life consistently expand the achievable trade space, and large packs provide additional range at the cost of increased mass and associated higher costs.

Keywords: battery electric vehicle; cell-to-pack; battery pack design; multi-objective optimization; techno-economic assessment; range analysis; battery lifetime; automotive engineering

Citation: Assyr Abdulle and Bernard Louis Koff. 2021. Multi-Objective Co-Design of Cell-to-Pack Battery Electric Vehicle Systems for Range, Cost, and Lifetime. *TK Techforum Journal (ThyssenKrupp Techforum)* 2021(3): 81–102.

Received: July-19-2021
Accepted: November-08-2021
Published: December-30-2021

1. Introduction

Design of battery electric vehicles (BEVs) is to a significant degree driven by battery-pack architecture. While design challenges in internal combustion vehicles relate mostly to engine performance, fuel economy, emission control, and drivetrain integration, in a BEV these functions are shifted to the pack. In other words, the traction battery is responsible for the production cost share, energy supply to the vehicle, curb mass and packaging, charging characteristics, thermal behavior, and durability [1–3]. Hence, the choice of a pack is not a secondary packaging consideration but a first-order decision of the system level.

Selection of the architecture becomes necessary because there is no direct transfer of electrochemical cell metrics to vehicle metrics. Gravimetric and volumetric density represent the cell performance in laboratory conditions. However, to convert an electrochemical cell into a pack it is necessary to provide an enclosure, interconnection elements, monitoring electronics, thermal contacts, protection circuits, and others. These components reduce density values and affect the correlation between pack capacity and vehicle performance [4–6]. In other words, a higher-density cell does not automatically imply a more efficient architecture.

The challenge of converting cell properties into vehicle performance has become more critical recently owing to wider adoption of BEVs. Customer satisfaction relies heavily on affordable pricing, sufficient range, convenient recharging process, and reliability of the battery pack [7–9]. However, despite considerable reduction in costs, battery packs continue to constitute one of the costliest vehicle parts [10–12]. This implies that a decision resulting in added nominal capacity but also increasing mass and/or cost may improve one parameter at the expense of reducing other parameters.

The industry's transition from modular layouts to cell-to-pack (CTP) and integrally structured packs is caused by these system-wide factors. Elimination of structural and intermediate layers is beneficial for packaging efficiency, battery mass reduction, and manufacturing cost [4,5]. All these factors affect not only the pack architecture but also the range and economics since the mass of the battery has direct impact on load energy demand and indirect impact on cost per kilowatt-hour. As such, the degree of integration is one of the design variables affecting vehicle performance.

The role of thermal design in defining battery lifetime is another aspect requiring an integrated approach. The battery's temperature defines its efficiency, power capabilities, aging rate, and safety margin [13–15]. The thermal load depends not only on battery chemistry but also on cell layout, cooling surfaces, structural density, and operating conditions. Cold temperature reduces battery power and may cause harmful reactions while hot temperatures enhance aging processes and increase risks of safety threats [16–18]. Hence, these factors should be considered simultaneously with the battery design.

Finally, lifetime is another factor that creates dependencies among the pack parameters. Cell lifetime is affected by throughput, DoD, temperatures, charge/discharge rate, and calendar exposure [19–21]. While increased capacity improves energy flow per kilometer, the total acquisition cost will also increase. Thus, a more cost-efficient design might have higher energy consumption per kilometer due to insufficient throughput. Hence, the task is not about maximizing number of cycles but selecting a suitable architecture that enables sufficient range and acquisition and lifetime costs.

Most concepts consider battery capacity as a single design parameter and evaluate a concept based solely on range. Such an approach works in limited settings but becomes insufficient if the format, integration level, battery capacity, and lifetime are taken into account. A battery pack with relatively high gravimetric/volumetric performance can become disadvantageous if the constraints on mass, energy fraction, and degradation cost are applied. Conversely, a design with lower gravimetric performance can be preferable in terms of range/cost/lifetime ratio in certain cases.

The current study addresses the problem by formulating a discrete co-design approach for BEV systems using cell-to-pack batteries. The approach evaluates a set of concepts characterized by year, cell format, installed energy, integration level, charging capabilities, and cycle life. Then the approach calculates mass and volume of pack, usable energy, range through the mass-specific energy consumption function, and lifetime value through total distance and degradation cost. The study deliberately considers the concept selection problem without copying one specific manufacturer platform but providing a numerical basis for comparison of alternative battery pack architectures.

Technically, the main research question is whether it is possible to choose a preferred battery pack based on nominal battery capacity or range, acquisition cost, and lifetime cost must be considered simultaneously. This paper contributes to this question by making three moves. First, it compiles a battery and vehicle models based on the literature data. Second, it evaluates the full design space comprising of 864 concepts and selects four cases according to 2025 and 2030 technology scenarios. Finally, it presents the results numerically to enable direct analysis of integration level, format, and capacity effects by manufacturing/automotive engineers.

2. Literature Related to Co-Design of BEV Packs

Past work related to this paper falls broadly into five areas of related research. The first of these relates to benchmarking of production BEVs by vehicle-level comparison. Studies of this type establish the performance envelope of different models, examine the relationship between pack size and weight versus real-world range, and demonstrate that the evaluation of battery energy must consider the vehicle category and operational context [22,23]. These works provide valuable insight into realistic expectations for BEVs, but comparative benchmarking does not identify which architecture choice might be made under various competing factors.

The second stream of research is concerned with battery costs, manufacturability, and economy-of-scale effects. Various studies projecting future battery prices have demonstrated that manufacturing yield and pack assembly efficiency have a large influence on pack costs [24,25]. In addition, strategic forecasts have emphasized the importance of reducing battery cost to ensure BEV competitiveness [9,11,12]. However, pack cost per kilowatt-hour is not always the only consideration in the selection process since low-cost batteries can be disadvantageous in terms of their influence on structural space requirement and curb weight, or lifetime.

The third area of interest involves electrochemical ageing of batteries and methods of predicting state of health, internal resistance changes, and lifetime. Electrochemical and diagnostic work has identified major ageing modes and created predictive techniques for quantifying residual capacity, resistance increase, and lifetime [26]. Further, work on battery management systems (BMS) has highlighted the importance of accurate estimation of state-of-charge, charge control strategy, and energy usable by the pack [27–29]. While crucial to pack design, the information derived here cannot be easily correlated with acquisition cost and driving range.

The fourth stream includes topics relating to thermal management and fast charging. Thermal management influences battery power capability, rate of degradation, charge acceptance, and abuse tolerance. Low temperatures can impair available power, while high temperatures and localized heating can promote faster ageing and thermal runaway events. When dealing with cell-to-pack architectures, the thermal problem is inherently linked to cell format and integration because of differences in heat dissipation and mechanical packaging resulting from the absence of modules and location of cooling plates.

The fifth area involves multi-objective optimization approaches. Methods such as Pareto ranking, distance-to-ideal ordering, and sensitivity analysis are used to differentiate dominated solutions from interesting trade-offs [30–32]. Engineering applications in electric vehicles include studies on power management, charging infrastructure, and hardware components [33–35]. Despite the prevalence of the latter, most of the studies related to BEV packs continue to assume that the battery is described solely by its capacity, with other aspects not explicitly incorporated.

There is clearly a technical gap in the literature that this paper seeks to address. Benchmarking, cost projections, electrochemical studies, and multi-objective approaches have been well-covered by the research community in the context of BEVs. There have been few efforts to create compact design calculations capable of returning numerical estimates of range, battery cost, and degradation costs per kilometre for multiple pack architectures in consistent vehicle context. Such work has now been accomplished in the present effort by evaluating a finite number of pack architectures under consistent vehicle assumptions.

3. Methodology

3.1. Design Variables and Case Definition

The battery system is represented using an architecture-selection approach involving the following six decision variables: technology year, cell format, gross pack energy, cell-to-pack integration factor, charging C-rate, and cycle life. The technology years correspond to two cases representing near-term and medium-term scenarios (2025 and 2030). There are three cell formats, cylindrical, prismatic, and pouch. Gross installed energy is discretized

using four values: 55, 65, 75, and 85 kWh. Cell to pack integration is captured using a multiplicative factor $\psi \in \{1.00, 1.05, 1.10, 1.15\}$. The charging rate is defined as $C_{\text{ch}} \in \{2.0, 3.5, 5.0\}$ h^{-1}. Cycle life is taken as $N_{\text{cyc}} \in \{1500, 2000, 2500\}$.

This produces a design space containing

$$2 \times 3 \times 4 \times 4 \times 3 \times 3 = 864$$

potential designs. The aim is not to replicate the catalogue of a particular manufacturer but to construct a representative design space based on literature and realistic assumptions.

Figure 1 illustrates the chain of calculation used in the analysis presented in the manuscript. The calculation process starts with discrete architectural selections and proceeds through cell-pack translations, vehicle-level constraints, and Pareto screening. This illustration is helpful since it clearly shows how the resulting selected pack is only produced after the energy, mass, volume, cost, charging, and lifetime data are calculated in precisely the same way.

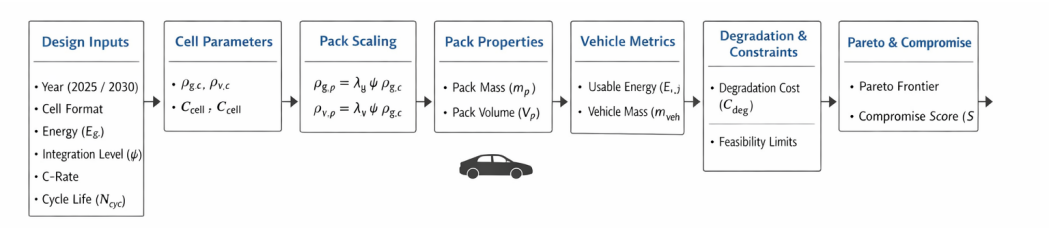

Figure 1. Model calculation workflow.

The physical unit represented by the model is a floor-mounted cell-to-pack battery system, shown in Figure 2. Figure 3 then summarizes the discrete catalogue from which the 864 candidates are assembled.

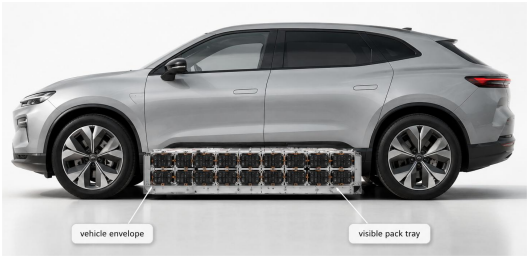

Figure 2. Cell-to-pack vehicle package.

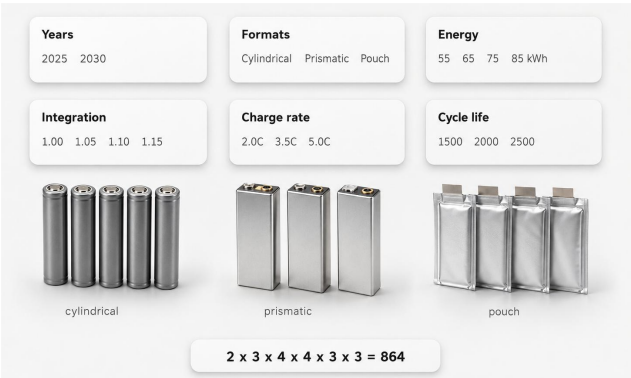

Figure 3. Discrete pack-design catalogue.

Both figures have their purpose. The first image shows the architectural artifact that is analyzed, whereas the second one tells us that the study under discussion does not

consider only the battery energy but also the timing of the technologies used, their formats, integration, charge rates, and lifetimes.

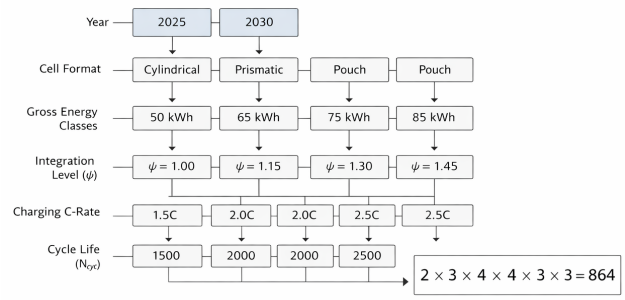

Figure 4. Design-space matrix.

Figure 4 helps better understand the math of 864 designs' combination. In this figure, each row represents a decision dimension, and the number of possible combinations is provided by multiplication on the bottom of the figure, which implies that all combinations are considered, not the selected few.

3.2. Battery Parameterisation

Example cell-level density and cost figures are used, based on past BEV and battery research, alongside reasonable assumptions derived from literature regarding near-term improvements [6,24,25]. Table 1 provides a summary of these parameters.

Table 1. Cell-level parameter assumptions used in the case model.

Year	Cell format	Gravimetric density (Wh/kg)	Volumetric density (Wh/L)	Pack cost (EUR/kWh)	Cycle-life set (cycles)
2025	Cylindrical	325	875	120	1500, 2000, 2500
2025	Prismatic	230	550	110	1500, 2000, 2500
2025	Pouch	283	700	115	1500, 2000, 2500
2030	Cylindrical	325	1000	92	1500, 2000, 2500
2030	Prismatic	285	990	85	1500, 2000, 2500
2030	Pouch	323	1000	89	1500, 2000, 2500

Numerical Table 1 creates the asymmetry behind subsequent findings. In the scenario of 2025, cylindrical cells are the most dense option gravimetrically, whereas the prismatic cells start off with a lesser density but higher cost, while the assumptions for the year of 2030 lessen the cost burden on prismatic cells. Hence, Table 1 reflects the realistic tradeoff between weight and cost, where the cheapest cell format is not necessarily the least heavy one, and vice versa.

Figures 5, 6, and 7 illustrate each cell parameter separately to allow analysis without overcrowding the graphs.

Gravimetric and volumetric densities of battery packs can be calculated based on the cell level ones as

$$\rho_{g,p} = \lambda_g \psi \rho_{g,c}, \tag{1}$$

$$\rho_{v,p} = \lambda_v \psi \rho_{v,c}, \tag{2}$$

where $\lambda_g = 0.50$ and $\lambda_v = 0.45$ represent the reference conversion from cell to pack. This accounts for the energy lost due to the non-cell structures and cooling of the cell-to-pack system [4,5,13]. In Eqs. (1) and (2), the integration factor is explicitly written out. An increase in ψ does not increase the chemical energy; rather, it increases the fraction of energy in the cell available after inclusion of enclosure, interconnects, cooling, and structures.

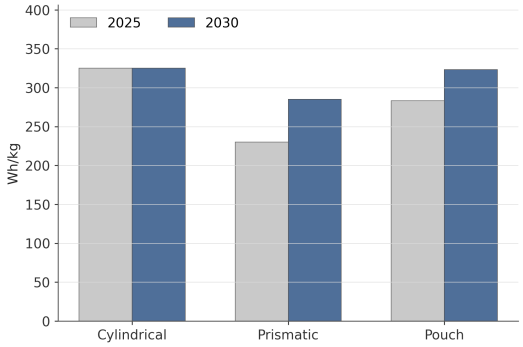

Figure 5. Cell gravimetric density.

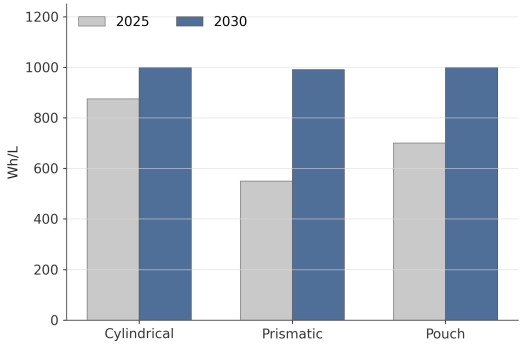

Figure 6. Cell volumetric density.

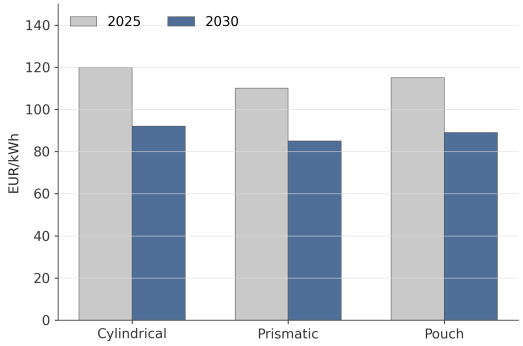

Figure 7. Pack-cost assumption.

The separate panels explain why the latter optimum is far from trivial. A high gravimetric-density value makes it easier to achieve feasibility of mass, high volumetric density helps maintain package volume, and low cost reduces both acquisition cost and degradation cost per kilometre. The design chosen needs to optimise on all three inputs instead of just one.

Figures 8, 9, and 10 add compact technical panels with the same set of inputs. This extra information is included because it shows numerical values of density and cost assumptions prior to their translation into pack mass, volume, and economic value by the equations.

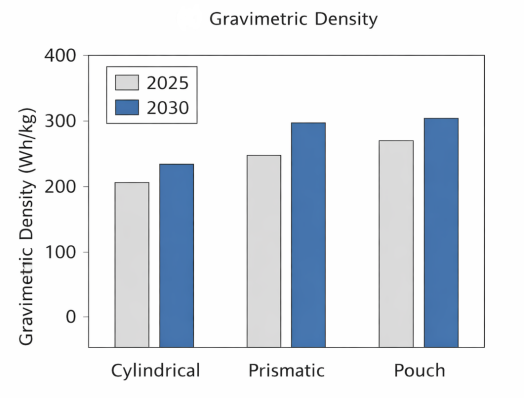

Figure 8. Gravimetric-density input panel.

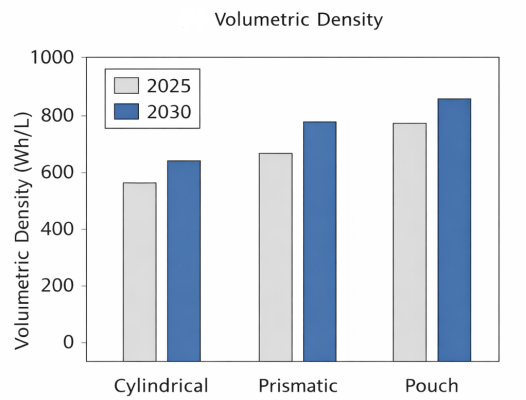

Figure 9. Volumetric-density input panel.

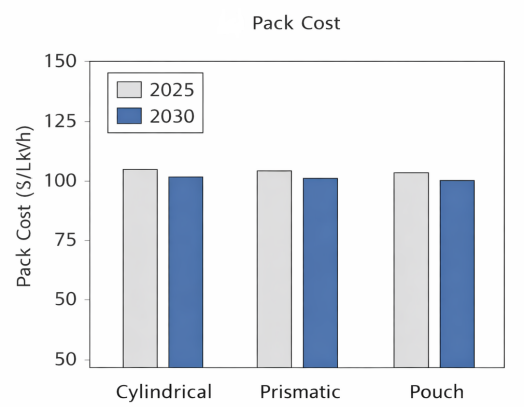

Figure 10. Pack-cost input panel.

It is observed from the three technical panels that the 2030 improvements assumed are not equally applicable across all formats. The prismatic density shows significant improvement, and the 2030 cost position is the lowest for prismatic format. This is why prismatic batteries become increasingly competitive over time despite being linked to the largest-range battery.

3.3. Usable Energy, Pack Mass, and Pack Volume

Installed energy, indicated by E_g, is measured in kWh. Usable energy is calculated through

$$E_n = \eta_u E_g, \tag{3}$$

where $\eta_u = 0.9266$ is the gross-to-net factor adopted for the reference case. This equation separates installed energy from usable energy because the driver experiences the net operating window, not the nominal pack label. Pack mass and pack volume are then

$$m_b = \frac{1000E_g}{\rho_{g,p}}, \tag{4}$$

$$V_b = \frac{1000E_g}{\rho_{v,p}}. \tag{5}$$

Eqs. (4) and (5) serve as the primary link between cell technology and car packaging. In case of fixed energy class, greater density decreases the mass and volume of the battery. If the density is constant, increase in E_g results in increased mass and volume. This is because nominal high energy cannot be evaluated without feasibility studies.

3.4. Vehicle-Level Energy Consumption and Range

The battery pack is modeled in combination with an electric crossover representative of the C-segment using a mass-based energy consumption model. The total vehicle mass is

$$M_v = M_0 + m_b, \tag{6}$$

where M_0 is the non-battery mass. Mixed-cycle electricity demand is then

$$e_v = e_0\left[1 + \beta\left(\frac{M_v - M_{\text{ref}}}{100}\right)\right], \tag{7}$$

where e_0 is the baseline electricity demand at the reference mass M_{ref}, and β is the mass sensitivity parameter. With Eq. (7), the more massive the battery, the less free it can be considered as a means for expanding the range: its mass will be able to contribute to increasing the specific energy consumption per 100 km. Calculated range turns out to be

$$R = \frac{100E_n}{e_v}. \tag{8}$$

Eq. (8) captures the key vehicle-level trade-off between range and consumption. Range depends on usable energy, while the denominator includes the mass factor associated with the very same battery. The form of Eq. (8) is intentionally concise. It does not substitute detailed drive cycle simulations, but retains the necessary interdependence for concept-level calculations: increased battery capacity will increase the usable energy capacity and the total mass, and hence energy consumption [5,22,23].

3.5. Battery Cost and Lifetime Value

Battery acquisition cost is modelled as

$$C_b = c_p E_g, \tag{9}$$

where c_p is the pack cost per annum for each particular format, year, and size from Table 1. The economic objective function, Eq. (9), assumes proportionality between the acquisition cost and installed energy such that low-cost cell types and low energy grades enter right away. The end-of-life travel distance is given by

$$D_{\text{EOL}} = N_{\text{cyc}}\phi R, \tag{10}$$

where the utility factor $\phi = 0.85$ accounts for conversion from nominal to effective cycle counts, allowing for the link between laboratory-like cycle life and vehicle service through

multiplication of every full cycle by the number of kilometres delivered by one battery cycle. The cost associated with degradation is

$$c_{\text{deg}} = \frac{C_b}{D_{\text{EOL}}}. \tag{11}$$

The lifetime performance index is purely economic, not electrochemical. The index reflects the ratio of pack costs per kWh to kilometers travelled over the useful life span of the battery. Thus, a pack design may be deemed undesirable due to high cost, low cycle life, short range, or any combination thereof.

3.6. Charging-Time Constraint and Feasibility Screening

Typical fast charge time to reach the 10–80% state of charge is

$$t_{10\text{–}80} = \kappa_{fc} \frac{0.70 E_n}{C_{\text{ch}} E_g}, \tag{12}$$

where $\kappa_{fc} = 1.25$ accounts for non-ideal charging behaviour and tapering. This expression is used as a screening relation, not as a detailed electrothermal charging model. A candidate design is retained only if

$$t_{10\text{–}80} \leq 25 \text{ min}, \tag{13}$$

$$m_b \leq 550 \text{ kg}, \tag{14}$$

$$V_b \leq 450 \text{ L}. \tag{15}$$

The three inequalities define the admissible engineering envelope. A configuration may be attractive in one objective but is removed before Pareto sorting if it cannot satisfy the charging, mass, or packaging limits of the vehicle class.

3.7. Multi-Objective Evaluation

Three objectives are considered:

$$\text{maximize} \quad R, \tag{16}$$

$$\text{minimize} \quad C_b, \tag{17}$$

$$\text{minimize} \quad c_{\text{deg}}. \tag{18}$$

Feasible designs undergo non-dominated sorting first. Then, a compromise score per year is calculated as the normalized Euclidean distance to the ideal point, defined as follows:

$$S_i = \sqrt{\frac{\hat{f}_{R,i}^2 + \hat{f}_{C,i}^2 + \hat{f}_{D,i}^2}{3}}, \tag{19}$$

with $\hat{f}_{R,i}$, $\hat{f}_{C,i}$, and $\hat{f}_{D,i}$ being the normalized distances of design i from the ideal values of range, cost, and degradation cost, respectively. Smaller scores correspond to better compromises. It is not meant to serve as a replacement for non-dominated sorting, but rather is used as an additional measure following the non-dominated sorting procedure to choose one balanced design with equal weights on the three objectives.

This computation can thus be done in four auditable steps: specification of the discrete architectural set, conversion of individual cell characteristics into aggregate weight and volume, evaluation of range and lifetime cost, and partitioning into infeasible, non-dominated, and compromise ranked designs. As each step involves explicit formulas, the impact of any modelling decision can be traced back to its input data.

4. Case Study Setup

The specific example concerns the C-segment electric crossover. Assumptions employed in this case study are clearly specified so as to provide for audibility and reproducibility of results. They are shown in Table 2.

Table 2. Vehicle-level assumptions for the representative case-study vehicle.

Parameter	Value
Non-battery vehicle mass, M_0	1380 kg
Reference vehicle mass, M_{ref}	1600 kg
Reference electricity demand, e_0	13.6 kWh/100 km
Mass sensitivity coefficient, β	0.015 per 100 kg
Usable-energy factor, η_u	0.9266
Lifetime utilisation factor, ϕ	0.85
Cell-to-pack mass factor, λ_g	0.50
Cell-to-pack volume factor, λ_v	0.45
Maximum acceptable fast-charge time	25 min
Maximum pack mass	550 kg
Maximum pack volume	450 L

Table 2 ensures that the same vehicle class is used, making the comparison pack-centric. The mass constraint is critical, ensuring that an extremely large-capacity pack does not become feasible simply due to its ability to provide a large range. The volume constraint stands for the availability of underfloor packages, while the fast-charge constraint excludes extremely low charge-rate possibilities from being considered as practical BEV designs.

The full-factorial enumeration of the design space generates 864 possible architectures. Application of the hard constraints reduces this number to 747 feasible solutions. Since the charging time formula depends solely on the C-rate and the C-rates tested all meet the threshold constraint of 25 minutes, charging capability becomes a feasibility constraint rather than a criterion for the objective values. When objective duplicates generated through the C-rate are removed, there remain 249 unique feasible architecture-lifetime pairs for further Pareto analysis and comparison.

5. Results and Discussion

5.1. Feasibility Structure of the Design Space

Feasibility constitutes the first issue. Table 3 provides the percentage of feasible designs per year and cell format. For the ranges employed in this work, the screening criterion is pack mass; no design is excluded on the basis of pack volume or charging time.

Table 3. Feasibility summary across the full 864-candidate design space.

Year	Format	Feasible	Total	Feasible share (%)
2025	Cylindrical	144	144	100.0
2025	Prismatic	63	144	43.8
2025	Pouch	126	144	87.5
2030	Cylindrical	144	144	100.0
2030	Prismatic	126	144	87.5
2030	Pouch	144	144	100.0

From Table 3, one can see that feasibility differs between formats and time periods. Whereas the majority of 2025 prismatic family candidates is eliminated, almost all of that design space is recovered in 2030. This quantitative difference matters since the Pareto solutions in the latter scenario are defined not only by objective functions but also the set of feasible candidates according to the mass constraint.

As one might expect, the format-wise pattern is explained directly by the assumed gravimetric density values. All of the prismatic cells at 75 and 85 kWh capacity exceed the upper limit of 550 kg on the pack mass in 2025. Therefore, the fraction of feasible candidates for prismatic pack type falls to just 43.8%. Pouch cells remain feasible in most combinations, but half of the 85 kWh variants are discarded owing to the same pack mass restriction. Cylindrical cell types are feasible throughout the whole capacity range, because their mass efficiency is higher based on the adopted assumptions. In 2030, the gain in gravimetric density for the prismatic family regains most of the feasibility lost in the previous year; only heavy 85 kWh designs with low integration levels fail to satisfy the mass constraint. Therefore, the feasible region depends not only on the cell format but on its interplay with density, energy class and the vehicle mass limit.

The integration level is a third parameter that defines feasibility clearly. Increasing the pack integration factor from $\psi = 1.00$ to $\psi = 1.15$ leads to a decrease in the pack mass by 13.0% in all formats, as it is proportional to ψ in this formulation. In the same time, the pack range is increased by a small fraction of 0.9%-1.2%, with degradation cost per kilometer reduced correspondingly. Therefore, higher integration level improves all three evaluated objectives without imposing any extra penalties in the current framework.

Figure 11 and 12 show the feasibility distribution for each technology case.

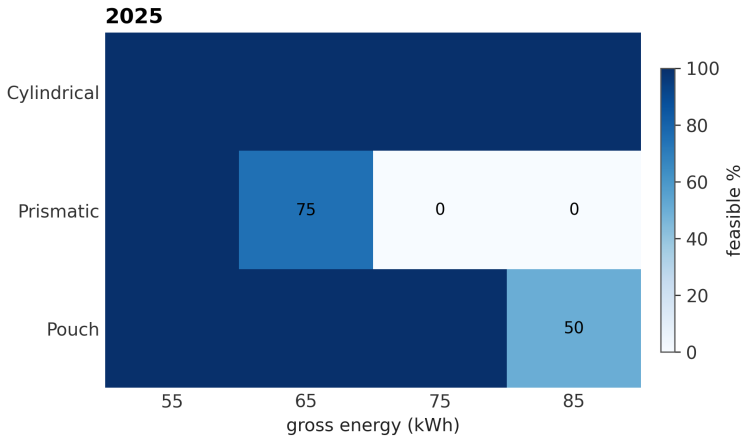

Figure 11. Feasible 2025 design share.

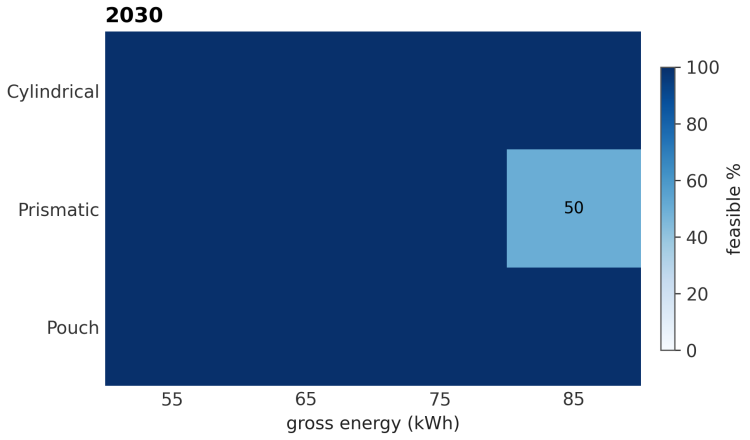

Figure 12. Feasible 2030 design share.

Technological advancements do not increase all numbers, but modify the design space shape, according to Figures 11 and 12. The major improvement is related to restoring feasibility of prismatic batteries for high energy classes, after which prismatic systems can become very competitive in the trade-off assessment.

The energy class view of the feasibility screening process is demonstrated in Figures 13 and 14. According to Figure 13, all prismatic batteries with large energy class values are cut off by mass constraints; while Figure 14 illustrates the effect of density improvements.

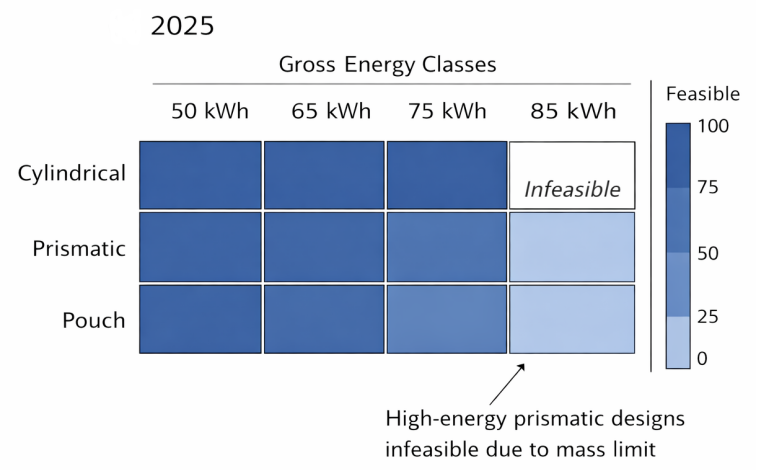

Figure 13. 2025 feasibility map.

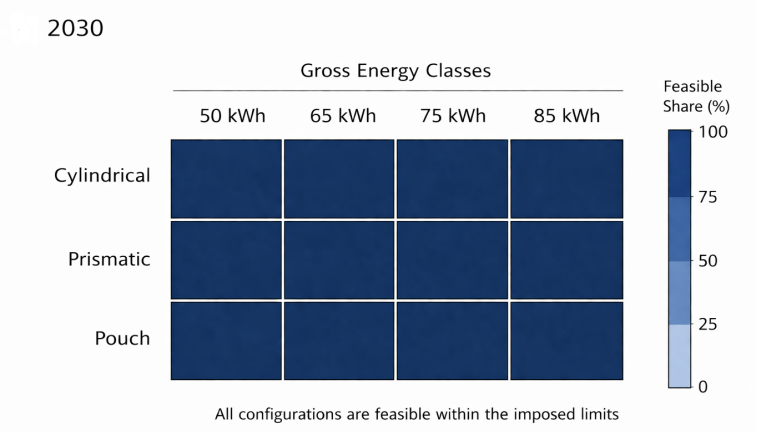

Figure 14. 2030 feasibility map.

The maps support the interpretation drawn from Table 3, namely that feasibility depends on pack mass but not a single penalty for a whole format. The critical point lies in the combination of high energy capacity and insufficient density or integration.

5.2. Pareto Frontier Maps By Year

As a result of combining 2025 and 2030 cases together, the non-dominated design pool consists of only 2030 technology due to its low cost and improved density. Thus, Pareto selection was done independently for each of these years. After removing the duplicate entries, there are 10 non-dominated designs in the 2025 case and 12 in the 2030 case.

All 2025 non-dominated designs feature the maximum integration and maximum number of cycles among the options used: $\psi = 1.15$ and 2500 cycles, respectively. In such a way, the next trade-off consists in energy class and format selection. Prismatic designs represent the lowest possible values of battery and degradation costs, while cylindrical and pouch packs demonstrate the maximal range. The analysis shows that the increase of pack capacity from 65 kWh to 85 kWh leads to an increase of range at the expense of higher capital expenses, with limited effects on degradation cost, considering that 2500 cycle lifetime has been taken into account.

The structure of the 2030 Pareto frontier is similar to the previous case, meaning that all non-dominated designs have the same maximum values of $\psi = 1.15$ and the same

number of cycles, 2500. However, as a consequence of the decreased cost and increased volumetric/gravimetric densities of prismatic cells in the 2030 case, their designs gain better positions on the map. Thus, even taking into account the fact that range is maximized in cylindrical/pouch packs, the position of prismatic cells becomes more prominent than in the case of 2025 technologies.

Figure 15 and Figure 16 illustrate range–cost trade-off for each year independently of one another.

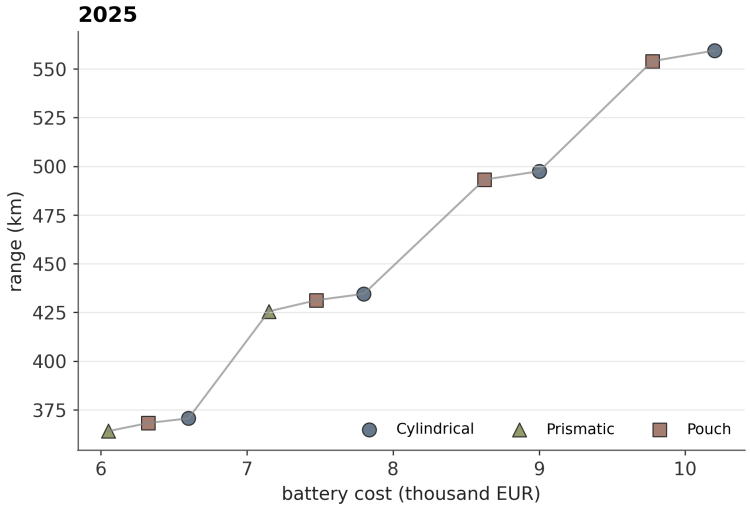

Figure 15. 2025 Pareto trade-off.

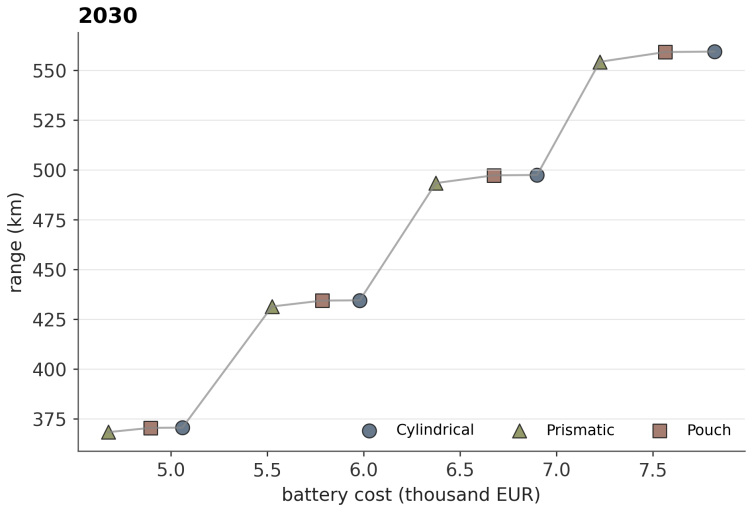

Figure 16. 2030 Pareto trade-off.

These frontiers demonstrate why the one-criterion analysis is not enough. It is important to remember that the high-end portion of the curve does not equal the minimum cost area. The designs that fall somewhere near the center of the frontiers will later become candidates for balanced packs.

The point-based visualizations presented in Figures 17 and 18 illustrate this principle. These figures are included here to demonstrate how certain formats fill the non-dominated range–cost area and what the cost of degradation is in these points.

It is clear from the point plots that the trade-off is a continuum and not just a two-valued choice. Although range improves towards the top-right region of the plots, improvement in range comes at an increase in the battery expense; hence, the preferred design can only come from the interior of the feasible frontier.

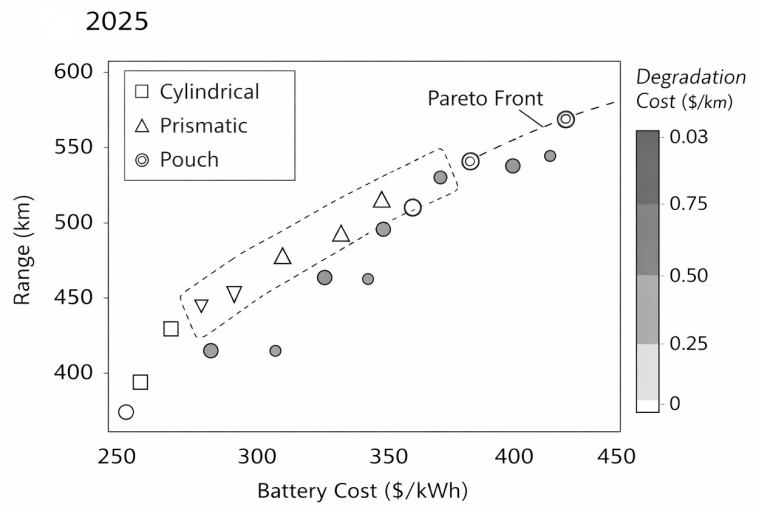

Figure 17. 2025 Pareto point map.

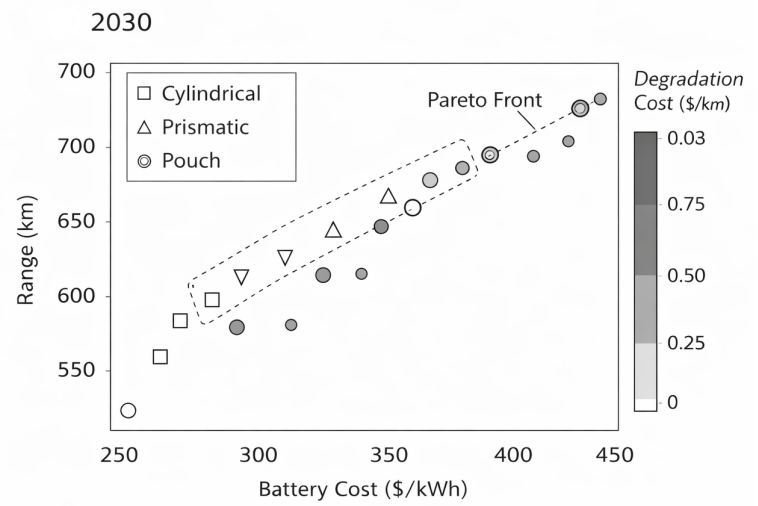

Figure 18. 2030 Pareto point map.

5.3. Compromise Ranking and Preferred Design Zone

The Table 4 below contains the most highly ranked Pareto fronts based on the weighted distance-to-ideal criterion defined by Eq. (19) every year.

As it can be seen from Table 4, the best candidates tend to cluster at high integration and high cycle life. It also needs to be mentioned that, the leading designs are not the same for the two periods under analysis, as for 2025 the optimal compromise is a 65 kWh prismatic pack, whereas in 2030 there is no need for sacrifice for obtaining an optimal compromise as it pertains to a 75 kWh prismatic pack.

In terms of 2025, the lowest compromise score is achieved with a 65 kWh prismatic pack with $\psi = 1.15$ and 2500 cycles. In particular, the pack offers a range estimate of 425.53 km and, in terms of battery cost and degradation cost, C_B =7150 EUR and C_D =0.0079 EUR/km, respectively. As one can see, the best 2025 compromise does not involve a lightest format and a largest battery; on the contrary, the optimal solution comes out of moderate energy class that performs well regarding cost and lifetime parameters.

When it comes to 2030, there is a new design with 75 kWh prismatic pack and the same parameters of integration level and cycle life. It gives an estimate of 493.40 km and a battery cost of 6375 EUR with degradation cost amounting to approximately 0.0061 EUR/km. Thus, compared to the leading compromise of 2025, the optimal compromise of 2030 allows obtaining 16% higher range, a battery cost decrease by about 11%, and degradation cost

decrease by approximately 23%. The corresponding energy class becomes greater (from 65 to 75 kWh).

Table 4. Leading compromise-ranked Pareto designs by year.

Year	**Format**	E_g **(kWh)**	ψ	N_{cyc}	m_b **(kg)**	R **(km)**	C_b **(EUR)**	c_{deg} **(EUR/km)**
2025	Prismatic	65	1.15	2500	491.49	425.53	7150	0.0079
2025	Pouch	65	1.15	2500	399.45	431.25	7475	0.0081
2025	Pouch	75	1.15	2500	460.90	493.17	8625	0.0082
2025	Prismatic	55	1.15	2500	415.88	364.03	6050	0.0078
2030	Prismatic	75	1.15	2500	457.67	493.40	6375	0.0061
2030	Prismatic	65	1.15	2500	396.64	431.43	5525	0.0060
2030	Prismatic	85	1.15	2500	518.69	554.29	7225	0.0061
2030	Pouch	65	1.15	2500	349.98	434.39	5785	0.0063

Compromise views for the specific years presented in Figures 19 and 20 show the position of the chosen designs against the non-dominated range-score relationship.

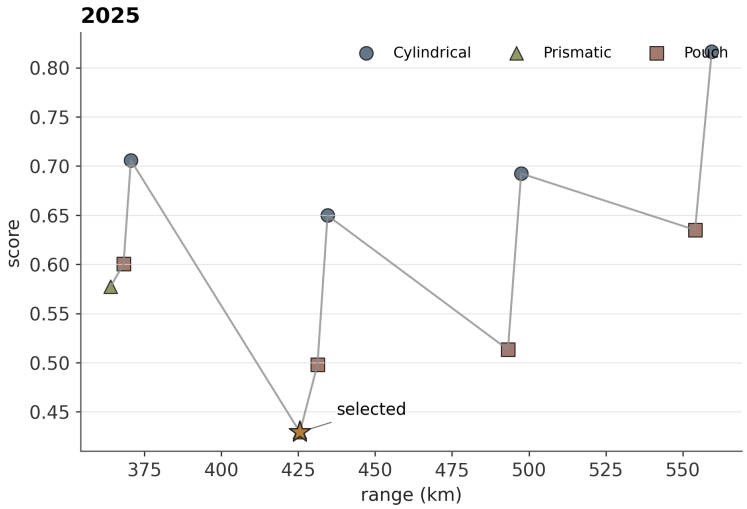

Figure 19. 2025 compromise ranking.

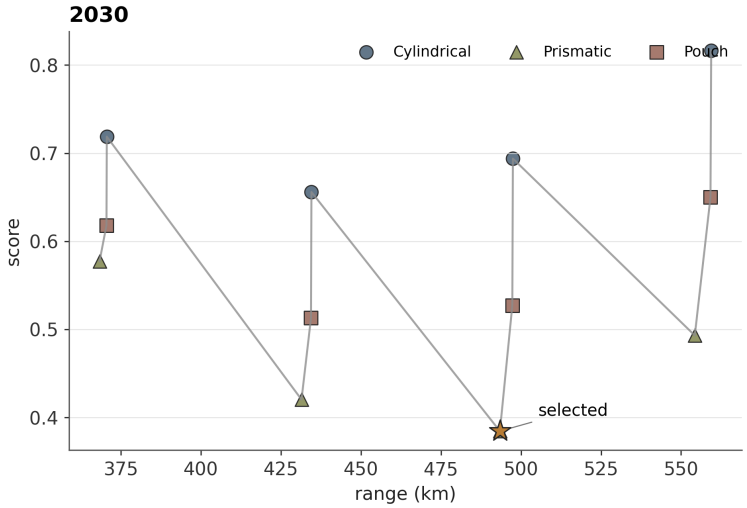

Figure 20. 2030 compromise ranking.

The selected compromise points are not on the edges with regard to the maximum range criterion. They are situated in middle classes in terms of energy, thus proving that the compromise function prioritizes energy efficiency over the installation of additional capacity.

The selected compromise points in Figures 21 and 22 serve as a proof as well, since the ranking is made clearly visible when the score and range distribution curve is taken into account. In this case, the optimal battery pack cannot be chosen by finding the point furthest to the right on the chart.

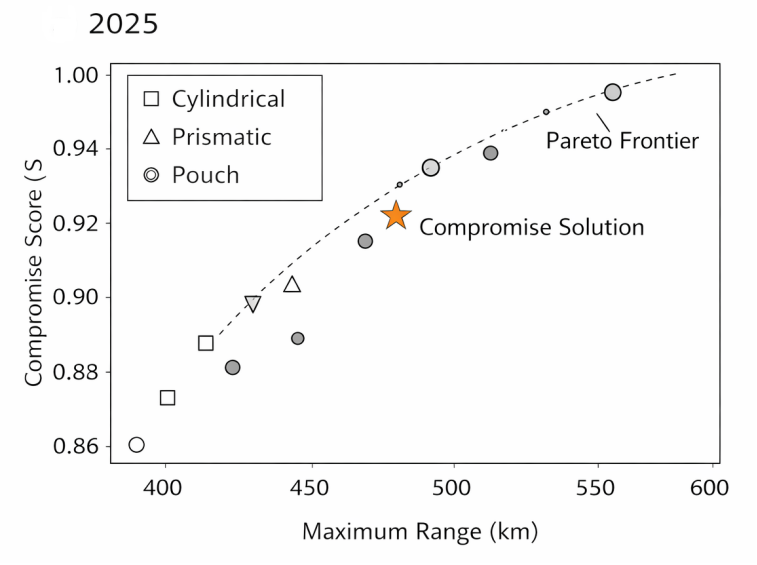

Figure 21. 2025 selected compromise point.

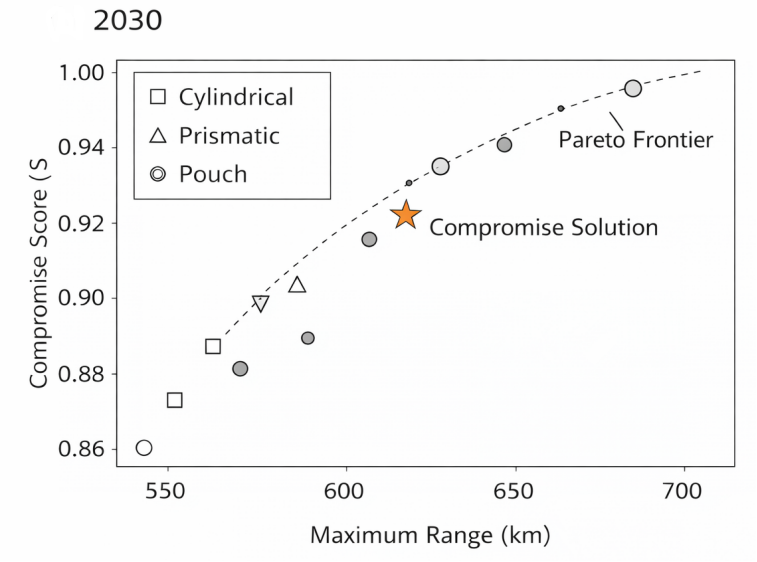

Figure 22. 2030 selected compromise point.

These points make clear the reasons behind moving from the 65 kWh prismatic choice for 2025 to the 75 kWh prismatic choice for 2030. The latter assumption allows for a higher-capacity battery pack due to the smaller penalties involved.

5.4. Objective-Specific Optima and Compromise Trade-Off

While compromise ranking seeks optimal balance, vehicle initiatives might value a particular objective over the other objectives. Table 5 provides objective-specific optima per year.

Table 5. Objective-specific best feasible designs by year.

Year	Objective	Format	E_g	ψ	N_{cyc}	R (km)	C_b / c_{deg}
2025	Maximum range	Cylindrical	85	1.15	1500	559.42	10200 EUR
2025	Minimum cost	Prismatic	55	1.00	1500	360.75	6050 EUR
2025	Minimum degradation cost	Prismatic	55	1.15	2500	364.03	0.0078 EUR/km
2030	Maximum range	Cylindrical	85	1.15	1500	559.42	7820 EUR
2030	Minimum cost	Prismatic	55	1.00	1500	365.63	4675 EUR
2030	Minimum degradation cost	Prismatic	55	1.15	2500	368.34	0.0060 EUR/km

Table 5 separates design intent from compromise selection. A range-led product would select a different pack from a cost-led product, and the minimum degradation-cost solution is again different. The practical value of the compromise result is therefore that it makes this separation explicit instead of hiding it behind one headline range value.

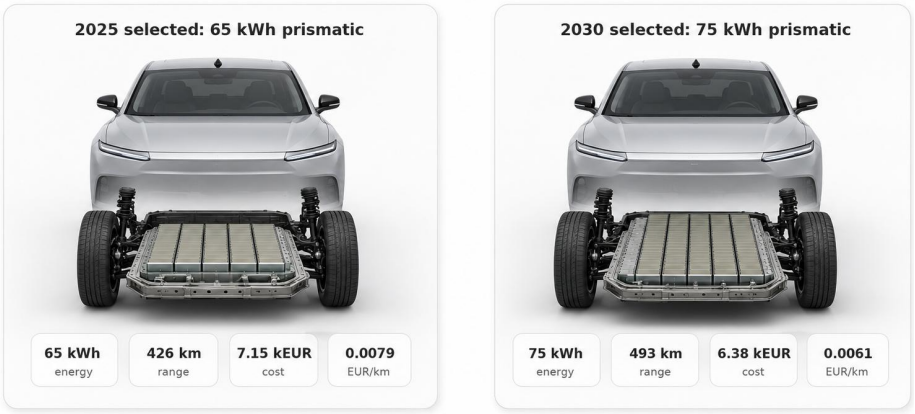

Figure 23. Selected cross-year packs.

Specifically, the objective-based outcomes illustrate a clear difference between designs for maximum range and for minimum cost of the battery pack. Regardless of year, maximum range is found in the 85 kWh cylindrical pack at $\psi = 1.15$, while minimum battery cost is achieved in the 55 kWh prismatic pack at $\psi = 1.00$. On the other hand, minimum degradation cost falls toward the low-energy side of the design space and features high integration combined with high cycle life. Hence, the compromise design can be seen as balancing between the extremes of maximum range for large packs and low cost for small packs. In 2030, the 75 kWh prismatic compromise pack has about 12% less range compared to the 85 kWh cylindrical maximum-range pack, while decreasing the cost of the pack by around 18.5%.

For an intuitive side-by-side comparison of the designs, Figure 23 illustrates the selected 2025 and 2030 packs. The comparison demonstrates that the advancement in 2030 is not a straightforward reduction in the acquisition cost with respect to the result in 2025, but allows for achieving balance in terms of high energy content, range, acquisition cost, and degradation cost.

Figure 24 presents a more comprehensive view by providing the objective-specific pathway of the selected packs in each year. The objective-specific pathways facilitate separating feasibility screening, Pareto ranking, and comparison on the frontier.

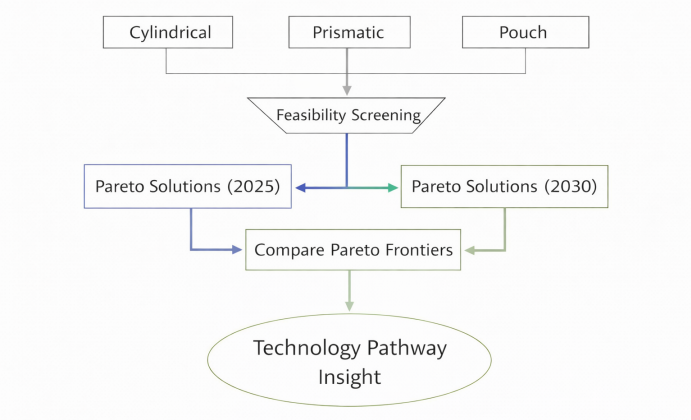

Figure 24. Cross-year comparison pathway.

The pathway approach is crucial for analyzing the technology impact. The gain made by 2030 will be considered as a single optimization task using the feasibility, Pareto, and compromise criteria as before 2025.

5.5. Sensitivity Analysis

In order to check the robustness of the best solution found for 2030 compromise designs, a sensitivity analysis based on the single parameter varying was applied to the case of the 75 kWh prismatic optimum.

Table 6. Sensitivity of the 2030 compromise-optimal design (75 kWh prismatic, $\psi = 1.15$, 2500 cycles).

Parameter change	Range change	Battery cost change	Degradation cost change
Base case	—	—	—
+10% vehicle specific consumption	−9.1%	0%	+10.0%
−20% cycle life	0%	0%	+25.0%
+10% pack cost per kWh	0%	+10.0%	+10.0%
Integration factor reduced from 1.15 to 1.00	−1.0%	0%	+1.0%
Usable-energy factor reduced from 0.9266 to 0.90	−2.9%	0%	+3.0%

Table 6 checks the robustness of the choice made for 2030. The effect of deterioration is asymmetric since durability loss has a larger influence on the cost associated with degradation compared to an increase in cost. Moreover, the effects of integration and energy efficiency of batteries are rather small.

Cycle life reduction turns out to be the most important source of sensitivity; a decrease of 12% of cycle life leads to an increase in the cost of degradation by 25%. For example, a 10% increase in the pack price will have the same effect on the cost of batteries and on the cost of degradation: their values will grow by 10%. At the same time, a 10% reduction of specific consumption will reduce range by 9.1%. However, a 5% reduction of the integration factor will lead to changes in range and cost of degradation of around 1%.

5.6. Insights on Format Design from the Results

In sum, the results indicate a preferred design region as opposed to a unique format that would dominate regardless of the weighting of different objectives. Specifically, the most effective region for 2025 consists of packs with energy classes of 65 kWh and above with both high integration levels and good cycle lives. In the case of 2030, the preferred design criteria remain unchanged, except the energy threshold of interest shifts to 75 kWh. High-range cylindrical, cost and lifetime-efficient prismatic and cost-efficient pouch batteries remain attractive formats at 2025 while prismatic batteries start gaining significant traction in 2030.

This analysis illustrates how battery-pack selection for an electric vehicle is a coupled design challenge as opposed to a standalone size choice. All the variables of gross energy, format and integration have a direct impact on pack mass, vehicle power consumption,

upfront battery cost and economic lifetime. After taking the interactions into account, the optimal solution ceases to be the largest battery pack but rather a design delivering an appropriate balance between range, cost and durability for the particular vehicle class.

An unambiguous conclusion based on the findings is that increased integration levels lead to better feasibility margins and improve the trade-off space systematically. The current range benefit might be minimal due to the mass-sensitive model. Still, the resulting improvement in pack mass and consequent reduction in degradation cost cannot be overlooked. This result confirms the practicality of the cell-to-pack and structurally integrated concepts described in the existing literature [4,5,13]. Integration is important not just as a means of achieving more pack capacity but as a system-efficiency tool.

Another interesting finding is how larger battery capacities translate into range improvements. While 85 kWh batteries offer the highest ranges, they do not dominate in the equally weighted compromise objective evaluation. The extra range comes with increased battery cost and, in certain cases, reduced feasibility margins. From the standpoint of product development, the 65–75 kWh battery size range seems to provide better results than 85 kWh batteries. Such an approach enables balancing between range leadership and design effectiveness.

The optimal battery format depends on the time scenario and its assumptions. While cylindrical cells dominate in 2025, they lose their competitive edge in 2030. Conversely, prismatic designs are more appealing as early as 2025 in terms of cost and cycle life objectives while pouch designs maintain their competitiveness in 2025 for some range-maximized batteries. The message is that there is no universal best battery format. Instead, the most appropriate format varies depending on the vehicle concept and underlying density and cost figures.

Figure 25 offers a concise visualization of the contribution made by cylindrical, prismatic and pouch battery formats to the useful design region. As expected, the figure demonstrates the conditional nature of format selection with cylindrical designs leading in range, pouch cells being competitive in selected high-range designs and prismatic cells excelling in terms of cost and lifetime evaluation.

Figure 25. Cell-format participation.

Figure 26 complements Figure 25 by identifying where the format-specific non-dominated sets overlap between 2025 and 2030. The overlap region highlights the designs that remain useful across both technology cases, while the year-specific regions show where density and cost improvements create new design opportunities.

The overlap view makes clear that progress in technology alters the location and the elements of the practical design space. Prismatic designs evolve towards a better compromise between 2025 and 2030 constraints. Cylindrical designs will remain in high demand if the range becomes a priority. Pouch cells will maintain their place if the power-to-energy ratio and thermal management become important.

Methodologically, the primary strength of the approach lies in its traceability. Cell-level density is converted to pack-level density, gross cell energy is converted to usable energy, pack mass is converted to vehicle consumption, and cycle lifetime is converted to a lifetime metric. Since these conversions are made explicitly, the whole model can be checked, altered, and replicated without recourse to proprietary information or proprietary software. Such property is quite valuable for conceptual-stage research, as general assumptions may be as informative as detailed models are.

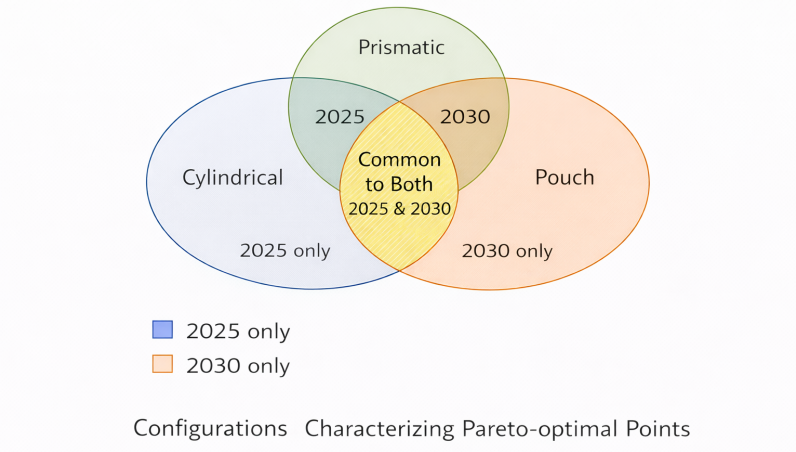

Figure 26. Format-overlap region.

Moreover, there are limitations of the model, which must be recognized when considering the results. Vehicle-consumption modeling assumes that there is no route- or weather-specific behavior and does not consider the effect of aerodynamics on performance. Charging is modeled with an approximation, without electro-thermo-hydraulic simulation. The lifetime metric does not separate cycle and calendar aging mechanisms and has no temperature history dependence incorporated. Also, the input data consists of design-level assumptions drawn from literature, not the measurements of a single production car. Such limitations do not invalidate any comparative results but limit the scope of conclusions.

However, there are numerous directions for further work. Drive cycles can be included into the analysis; floorplan geometry and crash safety concerns will have to be taken into account eventually. One could incorporate temperature history dependence of lifetime metrics and charging times or assign different weights to the compromise metric. Yet with all of these considerations, one conclusion seems inevitable – pack architecture should be selected based on a trade-off between energy, mass, cost, and cycle life.

6. Conclusions

The design problem stated as the research question in this paper is the choice between selecting an early-stage BEV battery pack by its nominal energy capacity alone and jointly by range, cost at acquisition, and cost per kilometre due to energy degradation during use. The quantitative solution to this problem is straightforward: nominal capacity is not enough. Although a pack with maximum nominal energy produces the largest estimated range in our studied case of C-segment crossover, it does not constitute the best trade-off among mass, cost, and value.

Our space of 864 designs reveals that feasible design points are first restricted by mass constraints before the volume and simplified charge rate criteria come into play. We filter out infeasible designs and remove charge rate duplications to arrive at 249 unique combinations of architecture and lifetime for Pareto analysis. This filtering process is far from being an auxiliary procedure since it eliminates excessive-energy packs that violate the pack-mass constraint of 550 kg and thus precludes the selection of physically unfeasible packs.

A compromise design with a 65 kWh nominal capacity of prismatic cells with $\psi = 1.15$ and a lifetime of 2500 cycles prevails among the designs in the 2025 technology case. It offers 425.53 km estimated range, 7150 EUR battery cost, and 0.0079 EUR/km degradation cost. For the 2030 technological scenario, a compromise design is a 75 kWh pack with similar cell-to-pack integration and cycle life. In this scenario, we obtain the following results: 493.40 km range, 6375 EUR cost, and approximately 0.0061 EUR/km degradation cost. Hence, advanced assumptions not only lead to lower costs; they also favour packs with larger nominal capacities while maintaining a desirable balance across three criteria.

We may derive three main practical insights from the results of this paper. Firstly, greater cell-to-pack integration helps create the feasible area of solutions and yields a moderate increase in range and degradation cost criterion. Secondly, lifetime remains critical since energy degradation cost per kilometre depends on service-equivalent distance. Finally, cell architecture is highly conditional; while cylindrical packs are successful in terms of estimated range, prismatic cells become superior in combination with higher cell-to-pack integration and better density and cost characteristics.

The architectures that will prove to be effective for the vehicle class under examination are those that allow to utilize energy efficiently rather than maximize the installed pack capacity. Therefore, the design recommendation implied in this study is to choose a pack design after its conversion to mass and volume, estimated range from energy capacity, and cost criterion from cycle life.

References

[1] Chan, C. C. (2007). The state of the art of electric, hybrid, and fuel cell vehicles. Proceedings of the IEEE, 95(4), 704-718.

[2] Ehsani, M., Gao, Y., Longo, S., & Ebrahimi, K. (2018). Modern electric, hybrid electric, and fuel cell vehicles. CRC press.

[3] Larminie, J., & Lowry, J. (2012). Electric vehicle technology explained. John Wiley & Sons.

[4] Nicoletti, L., Mirti, S., Schockenhoff, F., König, A., & Lienkamp, M. (2020). Derivation of geometrical interdependencies between the passenger compartment and the traction battery using dimensional chains. World Electric Vehicle Journal, 11(2), 39.

[5] Yun, L., Sandoval, J., Zhang, J., Gao, L., Garg, A., & Wang, C. T. (2019). Lithium-ion battery packs formation with improved electrochemical performance for electric vehicles: experimental and clustering analysis. Journal of Electrochemical Energy Conversion and Storage, 16(2), 021011.

[6] Thielmann, A., Neef, C., Hettesheimer, T., Döscher, H., Wietschel, M., & Tübke, J. (2018). Hochenergie-Batterien 2030+ und Perspektiven zukünftiger Batterietechnologien. Energiespeicher-Roadmap (Update 2017).

[7] Egbue, O., & Long, S. (2012). Barriers to widespread adoption of electric vehicles: An analysis of consumer attitudes and perceptions. Energy policy, 48, 717-729.

[8] Rezvani, Z., Jansson, J., & Bodin, J. (2015). Advances in consumer electric vehicle adoption research: A review and research agenda. Transportation research part D: transport and environment, 34, 122-136.

[9] Agrawal, M., & Rajapatel, M. S. (2020). Global perspective on electric vehicle 2020. International Journal of Engineering Research & Technology, 9(1), 8-11.

[10] Nykvist, B., & Nilsson, M. (2015). Rapidly falling costs of battery packs for electric vehicles. Nature climate change, 5(4), 329-332.

[11] Becker, T. A., Sidhu, I., & Tenderich, B. (2009). Electric vehicles in the United States: a new model with forecasts to 2030. Center for Entrepreneurship and Technology, University of California, Berkeley, 24(1).

[12] Henze, V. (2020). Battery pack prices cited below 100/*kwhforthefirsttimein*2020, *whilemarketaveragesitsat*137/kwh. Bloomberg New Energy Finance.

[13] Pesaran, A. A. (2002). Battery thermal models for hybrid vehicle simulations. Journal of power sources, 110(2), 377-382.

[14] Bandhauer, T. M., Garimella, S., & Fuller, T. F. (2011). A critical review of thermal issues in lithium-ion batteries. Journal of the electrochemical society, 158(3), R1-R25.

[15] Rao, Z., & Wang, S. (2011). A review of power battery thermal energy management. Renewable and Sustainable Energy Reviews, 15(9), 4554-4571.

[16] Jaguemont, J., Boulon, L., & Dubé, Y. (2016). A comprehensive review of lithium-ion batteries used in hybrid and electric vehicles at cold temperatures. Applied Energy, 164, 99-114.

[17] Feng, X., Ouyang, M., Liu, X., Lu, L., Xia, Y., & He, X. (2018). Thermal runaway mechanism of lithium ion battery for electric vehicles: A review. Energy storage materials, 10, 246-267.

[18] Wang, Q., Ping, P., Zhao, X., Chu, G., Sun, J., & Chen, C. (2012). Thermal runaway caused fire and explosion of lithium ion battery. Journal of power sources, 208, 210-224.

[19] Vetter, J., Novák, P., Wagner, M. R., Veit, C., Möller, K. C., Besenhard, J. O., ... & Hammouche, A. (2005). Ageing mechanisms in lithium-ion batteries. Journal of power sources, 147(1-2), 269-281.

[20] Barré, A., Deguilhem, B., Grolleau, S., Gérard, M., Suard, F., & Riu, D. (2013). A review on lithium-ion battery ageing mechanisms and estimations for automotive applications. Journal of power sources, 241, 680-689.

[21] Ecker, M., Gerschler, J. B., Vogel, J., Käbitz, S., Hust, F., Dechent, P., & Sauer, D. U. (2012). Development of a lifetime prediction model for lithium-ion batteries based on extended accelerated aging test data. Journal of Power Sources, 215, 248-257.

[22] Grunditz, E. A., & Thiringer, T. (2016). Performance analysis of current BEVs based on a comprehensive review of specifications. IEEE transactions on transportation electrification, 2(3), 270-289.

[23] Zubi, G., Dufo-López, R., Carvalho, M., & Pasaoglu, G. (2018). The lithium-ion battery: State of the art and future perspectives. Renewable and sustainable energy reviews, 89, 292-308.

[24] Berckmans, G., Messagie, M., Smekens, J., Omar, N., Vanhaverbeke, L., & Van Mierlo, J. (2017). Cost projection of state of the art lithium-ion batteries for electric vehicles up to 2030. Energies, 10(9), 1314.

[25] Schmuch, R., Wagner, R., Hörpel, G., Placke, T., & Winter, M. (2018). Performance and cost of materials for lithium-based rechargeable automotive batteries. Nature energy, 3(4), 267-278.

[26] Birkl, C. R., Roberts, M. R., McTurk, E., Bruce, P. G., & Howey, D. A. (2017). Degradation diagnostics for lithium ion cells. Journal of Power Sources, 341, 373-386.

[27] Lu, L., Han, X., Li, J., Hua, J., & Ouyang, M. (2013). A review on the key issues for lithium-ion battery management in electric vehicles. Journal of power sources, 226, 272-288.

[28] Hannan, M. A., Lipu, M. H., Hussain, A., & Mohamed, A. (2017). A review of lithium-ion battery state of charge estimation and management system in electric vehicle applications: Challenges and recommendations. Renewable and Sustainable Energy Reviews, 78, 834-854.

[29] Waag, W., Fleischer, C., & Sauer, D. U. (2014). Critical review of the methods for monitoring of lithium-ion batteries in electric and hybrid vehicles. Journal of Power Sources, 258, 321-339.

[30] Deb, K., Pratap, A., Agarwal, S., & Meyarivan, T. A. M. T. (2002). A fast and elitist multiobjective genetic algorithm: NSGA-II. IEEE transactions on evolutionary computation, 6(2), 182-197.

[31] Das, I., & Dennis, J. E. (1998). Normal-boundary intersection: A new method for generating the Pareto surface in nonlinear multicriteria optimization problems. SIAM journal on optimization, 8(3), 631-657.

[32] Marler, R. T., & Arora, J. S. (2004). Survey of multi-objective optimization methods for engineering. Structural and multidisciplinary optimization, 26(6), 369-395.

[33] Onori, S., Serrao, L., & Rizzoni, G. (2016). Hybrid electric vehicles: Energy management strategies (Vol. 13). London: Springer.

[34] Brenna, M., Foiadelli, F., Leone, C., & Longo, M. (2020). Electric vehicles charging technology review and optimal size estimation. Journal of Electrical Engineering & Technology, 15(6), 2539-2552.

[35] Coello, C. C. (2006). Evolutionary multi-objective optimization: a historical view of the field. IEEE computational intelligence magazine, 1(1), 28-36.